ASAR Wave Mode

- Validation of Reprocessing Upgrade

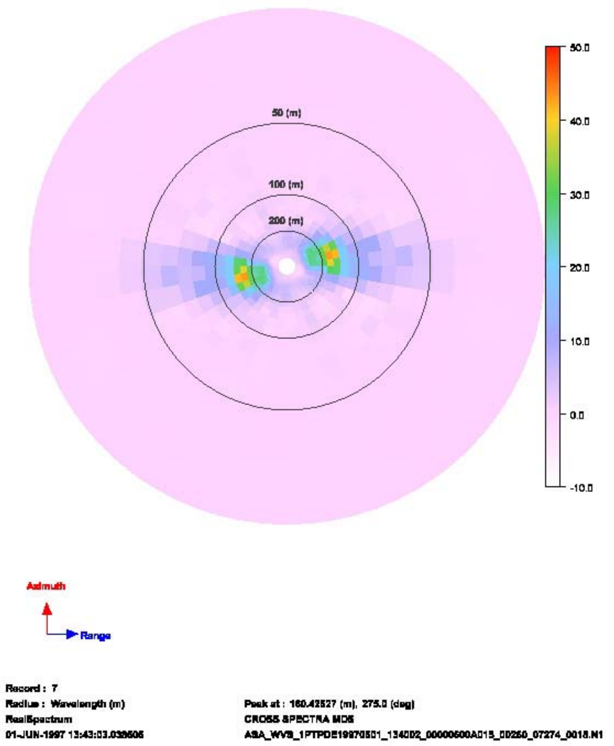

ESA ESRIN Contract No.: 17376/03/I-OL

ESA Technical Management: Betlem Rosich

Prime Contractor: Norut Informasjonsteknologi AS

Co-Investigator: BOOST Technologies

Project Manager: Harald Johnsen

Project: Long-Term Quality Assessment and Optimization of ASAR Wave Mode Products

Document Title ASAR Wave Mode Processing – validation of reprocessing upgrade			
Author(s) Harald Johnsen , Fabrice Collard			
Contractor ESA/ESRIN		**Contracting Ref** 17376/03/I-OL	
ISSN 1503-1705 **ISBN 82-7747-140-8**	**Document No.** 3/2006	**Document Type** IT-Rapport	**Status/Availability** Open D7
Date 15th March 2006		**Version** 1.0	**No. of Pages** 26
Keywords Envisat ASAR Wave Mode, Wave Spectra, Calibration and Validation			
Notices			
Distribution ESA			
Reviewed by Kjell-Arild Høgda		**Technical Responsible** Jan-Børre Rydningen	
Abstract/Summary The validation of the reprocessing of ASAR Wave Mode products at IFREMER is presented in this report. The geophysical validation of the ASA_WVS and ASA_WVW products are performed using collocated WAM and buoy data. The validation process consists of comparison with the original ESA products as well as comparison with collocated model and buoy data. Several months of WM data are used in the validation, where one month of data is usually around 35000 imagettes.			

CONTENT

1 INTRODUCTION

As part of the reprocessing of the Envisat ASAR Wave Mode archive at IFREMER, a major upgrade of the Level1 (WVS product) and Level2 (WVW product) processing algorithms were done. The description of the algorithm upgrades can be found in [B-9]. In this report the results of the validation of the reprocessed products against collocated WAM and buoy data are presented, as well as a comparison with the original WVS and WVW products.

1.1 ACRONYMS

ASAR = Advanced Synthetic Aperture Radar
SUM = Software Users Manual
SRD = Software Requirements Document

2 REFERENCE AND APPLICABLE DOCUMENTS

2.1 APPLICABLE DOCUMENTS

[A-1] Johnsen H., Engen G., Lauknes I., The ENVISAT ASAR Wave Mode Cross Spectra Algorithm - Software Requirements Document, NORUT Report ASAR-D6-NT-01, v. 1.4.0, Dec 2004.

[A-2] Johnsen H., Engen G., Høgda K.A., B. Chapron, F. Collard, ENVISAT ASAR Level 2 Wave Mode Product Algorithm Specification - Software Requirements Document, NORUT IT report IT650/1-01, v.2.2.9, Oct 2005.

[A-3] Johnsen H., Engen G., Lauknes I., The ENVISAT ASAR Wave Mode Cross Spectra Algorithm - Software User Manual and Installation Guide, NORUT Report ASAR-D16-NT-01, v. 1.4.0, Jun 2005.

[A-4] Johnsen H., Engen G., Høgda K.A., B. Chapron,, ENVISAT ASAR Level 2 Wave Mode Product Algorithm Specification - Software User Manual and Installation Guide, NORUT IT report IT650/3-01, v.1.2.2, Oct 2005

2.2 REFERENCE DOCUMENTS

[B-1] Chapron B., Collard F., Johnsen H., Engen G., “ASAR Wave Mode First Geophysical Results”, Proc. of Envisat Calibration Review, SP-520 Proceedings, ISBN 92-9092-830-1, http://www.envisat.esa.int/.

[B-2] Johnsen H., Engen G., Chapron B., "Validation of ENVISATASAR Wave Mode Level 2 Product", Proc. of Envisat Calibration Review, SP-520 Proceedings, ISBN 92-9092-830-1, http://www.envisat.esa.int/.

[B-3] Johnsen H., Engen G., Chapron B., Walker N., Closa J., " Validation of ASAR Wave Mode Level 2 Product", Proc. of ENVISAT Cal/Val Workshop, ESA SP-531 Proceedings, http://www.envisat.esa.int/.

[B-4] Johnsen H., Kerbaol V., “Technical Support for Global Validation and Long-Term Quality

Assessment and Optimization of ASAR Wave Mode Products: Specification of Parameters", Norut IT/Boost Technologies Note, November 2003.

[B-5] Johnsen H., Kerbaol V., "Technical Support for Global Validation and Long-Term Quality Assessment and Optimization of ASAR Wave Mode Products: Cycle Reports", Norut IT/Boost Technologies, http://www.boost-technologies.com

[B-6] Kerbaol V., Johnsen H., Chapron B., Rosich B., "Quality assessment of ASAR Wave Mode products based on regional and seasonal comparison with WAM model outpust", ERS/Envisat Symposium, 6-10 Sept. 2004, Salzburg

[B-7] Johnsen H., Engen G., Chapron B., "Validation of ASAR Wave Mode Level 2 product using WAM and buoy spectra", Proceeding Coastal & Marine Applications of SAR, 8-12 Sept., 2003, Svalbard, ESA SP-565.

[B-8] Johnsen H., "Wind and Wave Data Calibration and Validation Results", Norut IT Report IT750/2-2004 v1.1, January 2005.

[B-9] Johnsen, H., Collard F., "ASAR Wave Mode – Description of Reprocessing Upgrade", Report IT No:3/2005, v.1.1, October 2005

[B-10] Johnsen, H., "ASAR Wave Mode – Product Manual", Report IT No:1/2005, v.1.2, October 2005

3 THE ASAR WVS PRODUCT

From the long term monitoring and validation of the WVS product [B-4], [B-5], artefacts were observed in the image statistical parameters and azimuth cut-off parameter. Impacts of low frequency noise in the cross spectra were also observed. Based on these observations, the following upgrades of the ASAR Wave Mode WVS product and algorithm are implemented in the reprocessing chain at IFREMER [B-9].

a) improved computation of image statistics i.e. mean intensity, normalized variance, skewness, and curtosis

b) improved azimuth cut-off computation using the bi-section algorithm instead of the Newton iteration scheme

c) a new image detrending procedure, based on low pass filtering of the original SLC imagette

3.1 VALIDATION

1.3.2 COMPARISON WITH ORIGINAL ESA PRODUCT

In the following plots we compare some key parameters of the WVS product before and after the upgrade of the WVS processing.

a) Image Statistics

In Figure 1 we plot histograms of normalized image variance, skewness and curtosis extracted from the WVS product. The left plots are from the old WVS product, while the plots to the right are from the upgraded WVS product.

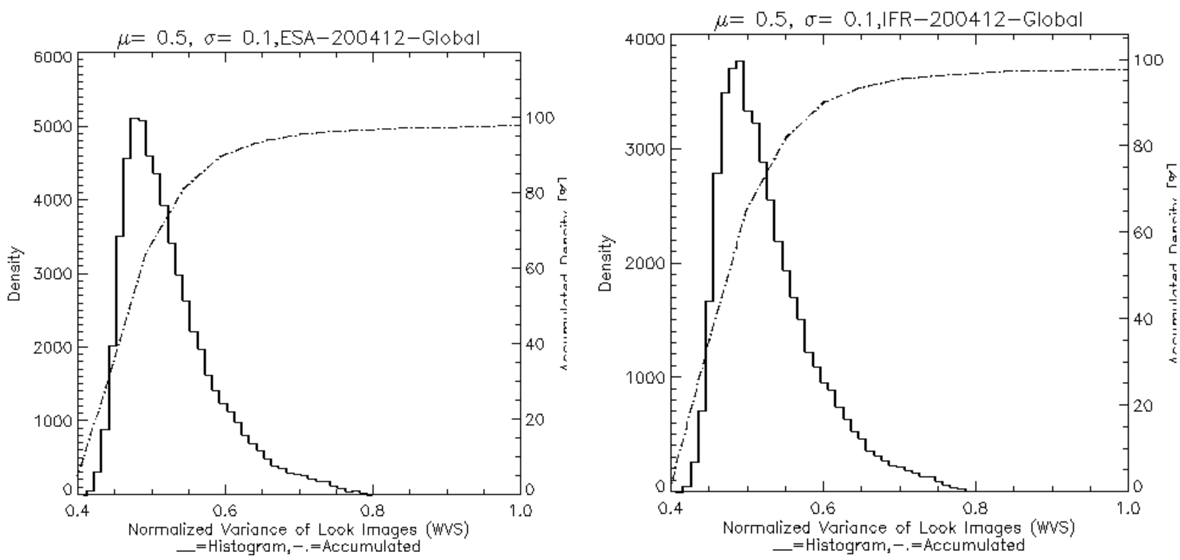

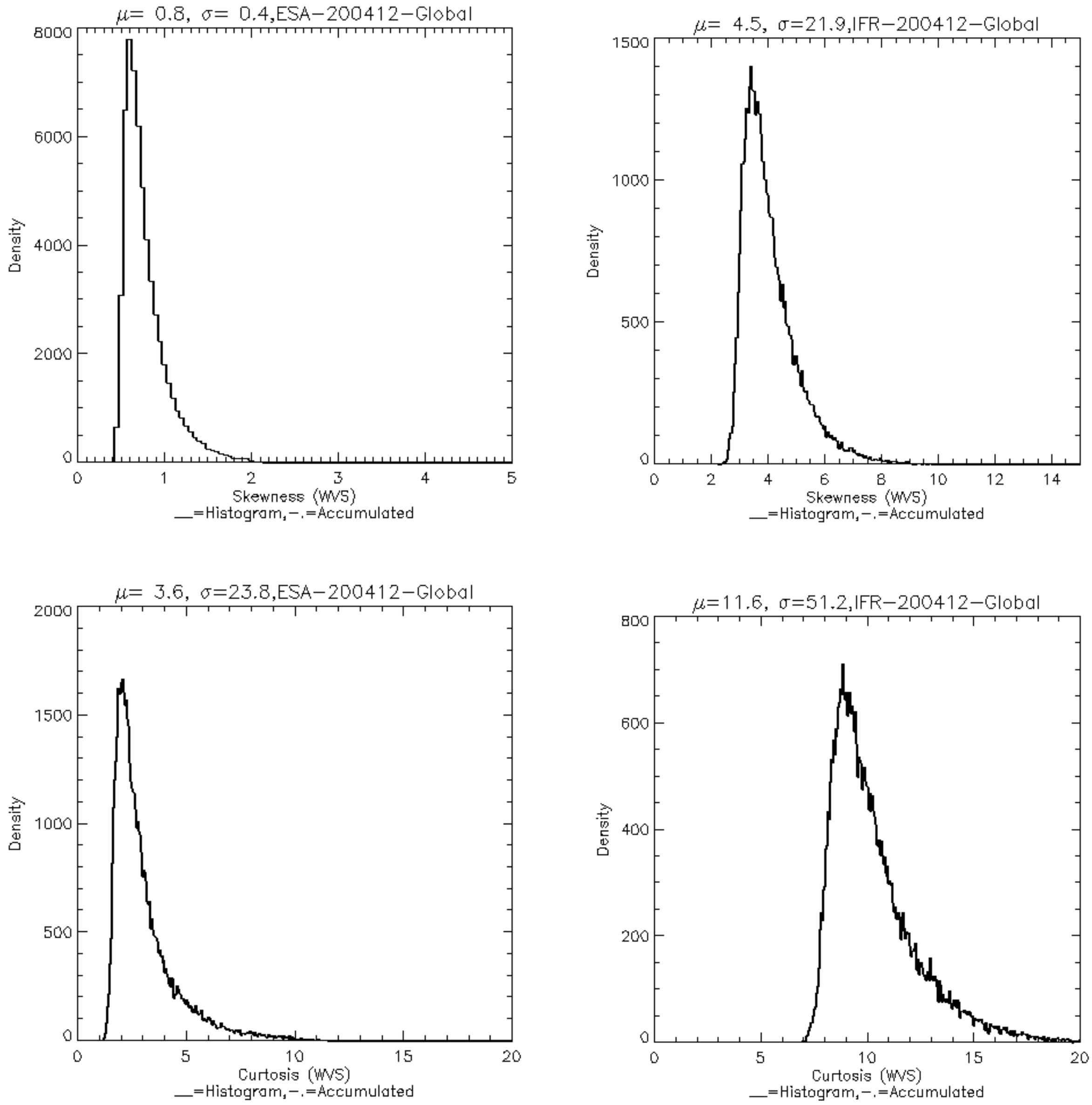

Figure 1: Histogram of normalized image variance (upper), squared skewness (mid), and curtosis (right) before and after the upgrading.

Figure 1 shows significant changes and improvements in the image statistical parameters stored in the WVS product, especially for the skewness and curtosis.

b) Azimuth Cut-Off

In Figure 2 we show the histogram of the azimuth cut-off parameter before and after the upgrade of the WVS processing.

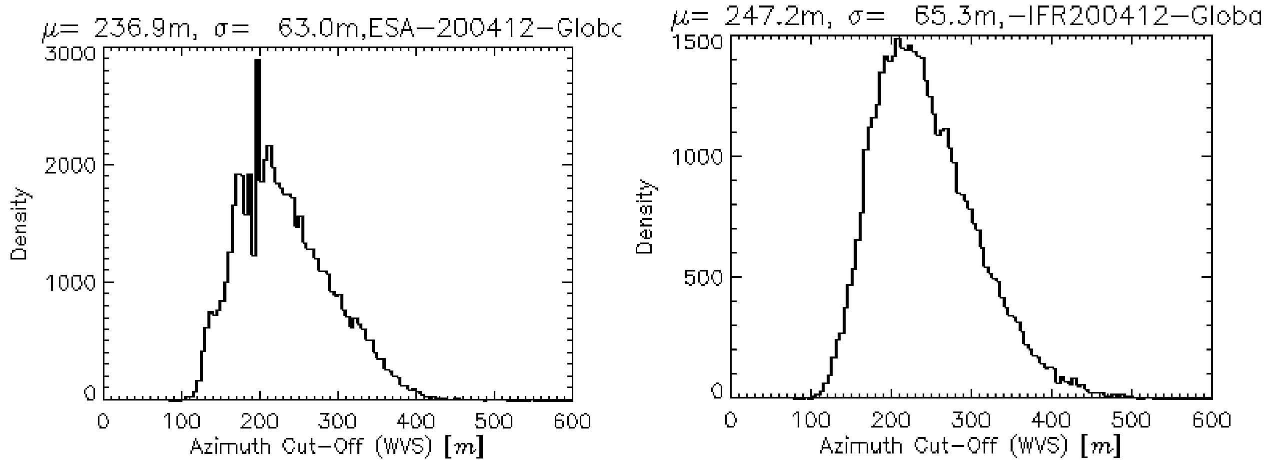

Figure 2: Histogram of ASAR WVS azimuth cut-off parameter before (left) and after (right) the upgrading of the WVS product.

Figure 2 shows a clear improvement in the estimation of the azimuth cut-off value, and the shape of the histogram is now similar to the new WVW azimuth cut-off (see Figure 21).

c) Detrending

The new detrending procedure is based on dividing the SLC imagette by a low-pass filtered version of the same imagette. This is similar to what was implemented in the first version of the Level 2 product [A-4]. The width of the low pass filter (trRemWidth) is a parameter to be defined in set-up processing file [A-3]. As an example, a width of the filter of 400m will filter out all wavelengths above 800m.

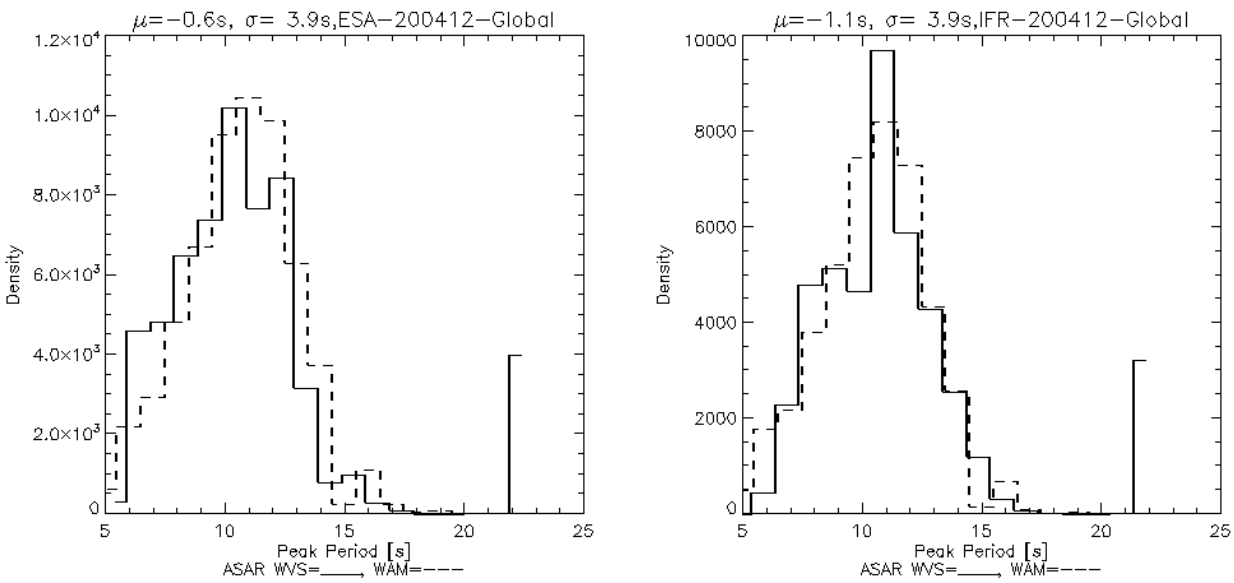

Figure 3: Histogram of ASAR WVS cross-spectra peak period (full line) before (left) and after (right) the upgrading of the WVS product. The dotted line shows the corresponding WAM histogram.

Figure 3 shows only a slight modification of the histogram. This is probably due to the specification of the width of the low-pass filter in the set-up file used in the reprocessing of the WVS product. If we set the filter width to 340m, which means we are filtering out all wavelengths above 680m or 21sec, the large peak in the histogram at high wave periods of Figure 3 would have been reduced. Plots like Figure 3 can be used to optimize the setting of the filter width in the processing set-up file (see Chapter 1.4.5).

1.3.3 COMPARISON WITH NUMERICAL WAVE MODEL

In the next plots a comparison against WAM parameters is presented.

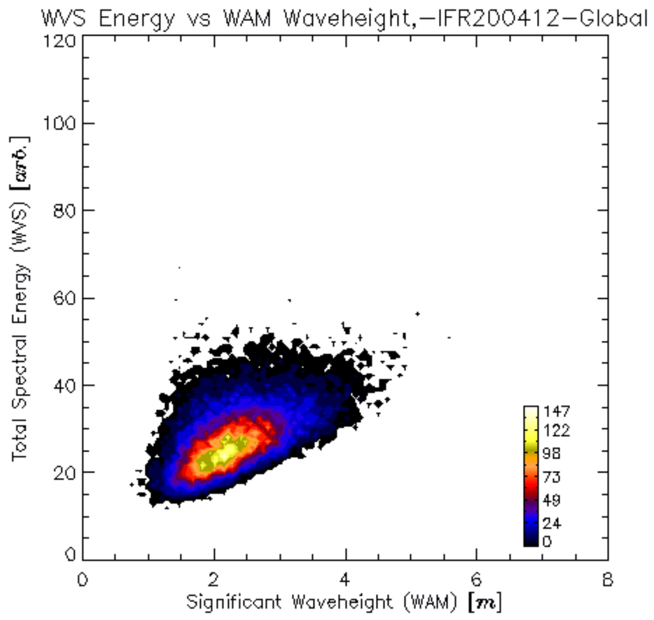

Figure 4: Total cross spectra energy versus ECMWF WAM significant waveheight.

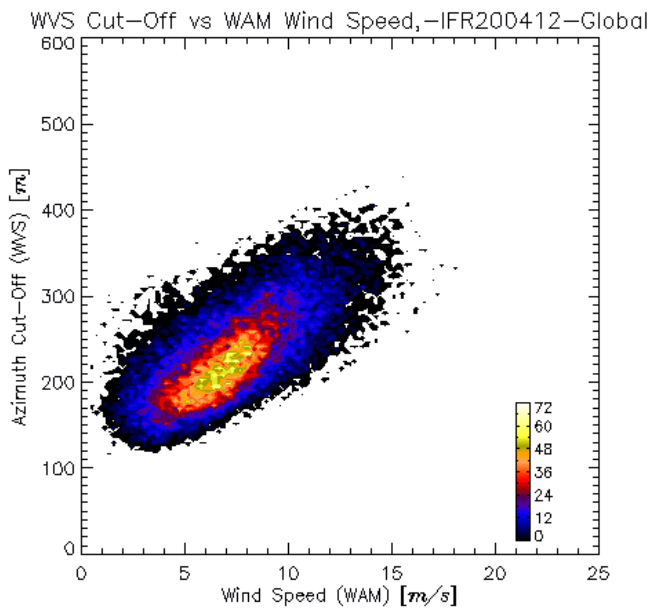

Figure 5: Azimuth cut-off versus ECMWF wind speed

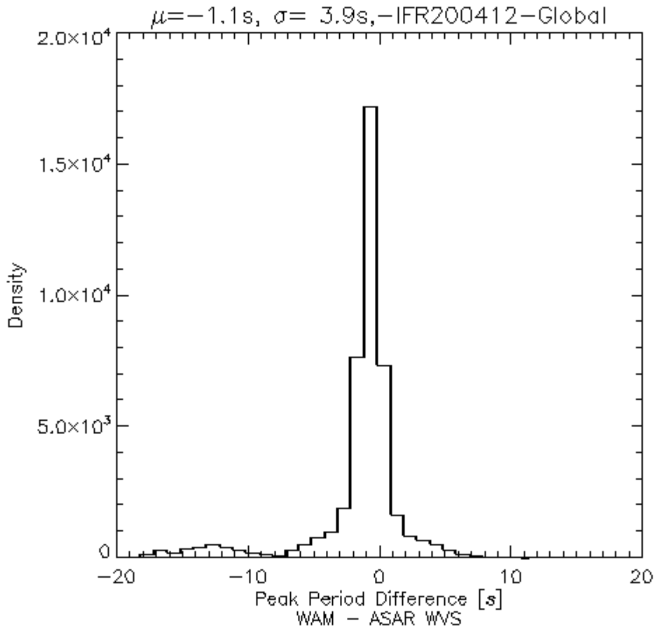

Figure 6: Histogram of the difference of WVS cross spectra peak period and ECMWF WAM peak period.

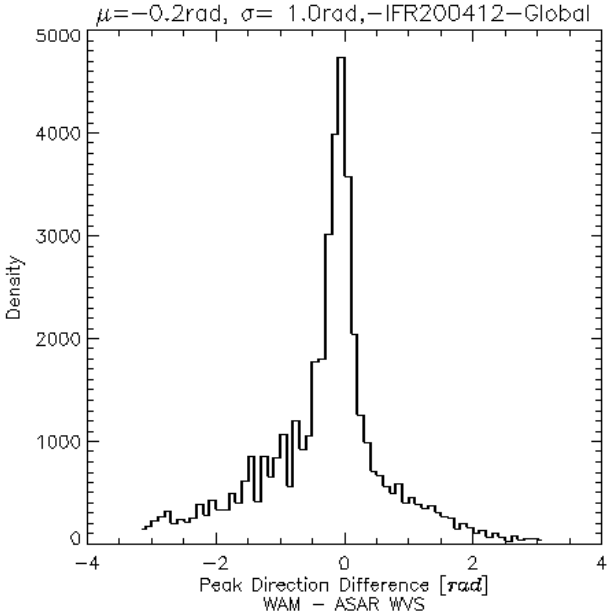

Figure 7: Histogram of the difference of WVS cross spectra peak wave direction and ECMWF WAM peak wave direction.

Figure 4 to Figure 7 show performance of the WVS parameters as expected. Compared to old WVS product, the most significant improvements is observed in the azimuth cut-off.

4 THE ASAR WVW PRODUCT

Based on the systematic long term validation of the WVW product [B-5] to [B-8] an upgrade of the Level 2 algorithm was developed and implemented at IFREMER/CERSAT. The major problems observed in the first version of the Level 2 algorithm are related to; - large number of non-physical spectra, - overestimation of mean period of swell, - overestimation of Hs, especially at low sea-state, - ambiguity in swell propagation direction at low SNR, - azimuth cut-off value
The solutions were found by; - detrending in spectral domain, - modification of the modulation transfer function at low wavenumbers, - improved SNR measure, -new ambiguity flag, and a new azimuth cut-off estimator.

Detrending:

The large number of non-physical specta was related to improper detrending of the imagette. An additional non wave feature removal is applied in the Fourrier domain of the image cross spectra by removing spectral contributions that are maximum at the cutoff frequencies (800m) and decreasing monotonically to higher wavenumbers. Example of improvement of the final wave spectra is shown in the Figure 8.

Ambiguity:

The ambiguity removal in the Level 2 processing is based on generating a symmetric and a anti-symmetric wave spectra by applying the modulation transfer function (MTF) on the real and imaginary parts of the cross-spectra, respectively. Then only those wave components in the symmetric spectrum with values above certain positive value in the anti-symmetric spectra are kept. However, it has turned out that the imaginary part of the cross-spectra has often a low SNR, which in combination with the MTF may produce ambiguities in the wave direction retrievals. We thus recommend to apply on the imaginary part of the cross-spectra a modified MTF that is thresholded to avoid noise amplification at low frequencies and a weighting function based on the ambiguous inverted wave spectrum. This improvement in ambiguity removal has a strong impact when several wave systems are present at the ocean surface since the imaginary part of the longer wave system might have an SNR lower than the some surrounding low frequencies or noise contribution. Additionally a new parameter (*ambiFac* instead of *signal-to-noise*) is used to assess the confidence flag of the swell inversion. The *ambiFac* is also stored in the spare field of the *OCEAN WAVE SPECTRA MDS* of the new Level 2 product.

Modulation Transfer Function:

It has further been observed that the actual SAR MTF tends to overestimate the swell at low wavenumbers. This has the double impact of reducing the relative importance of rather developed wind seas (in the range 100-200m) and overestimating the wavelength of swell systems. This artefact is due to the assumption that all spectral components of the wave spectrum are free propagating waves. This assumption is no longer valid for wavenumber lower than the spectral peak which are not propagating waves but effects of wave groupiness (limited number of waves within a group equivalent to a peak broadening in the spectral domain). We thus suggest to apply, on wavenumber lower than the peak for each single direction, the same transfer function as for the peak wavenumber.

Azimuth Cut-Off:

The new azimuth cut-off estimation is based on using a Gaussian roll-off function for the azimuth profile of the cross-correlation function. The iterative procedure for doing the minimization is based on the bisection algorithm.

Noise Correction:

The mean imagette intensity (or radar cross section) is corrupted by additive noise from quantization and thermal noise. A noise correction of the image intensity is performed based on a apriori based model of fraction of noise versus signal intensity developed by analyzing 26930 imagettes [B-9].

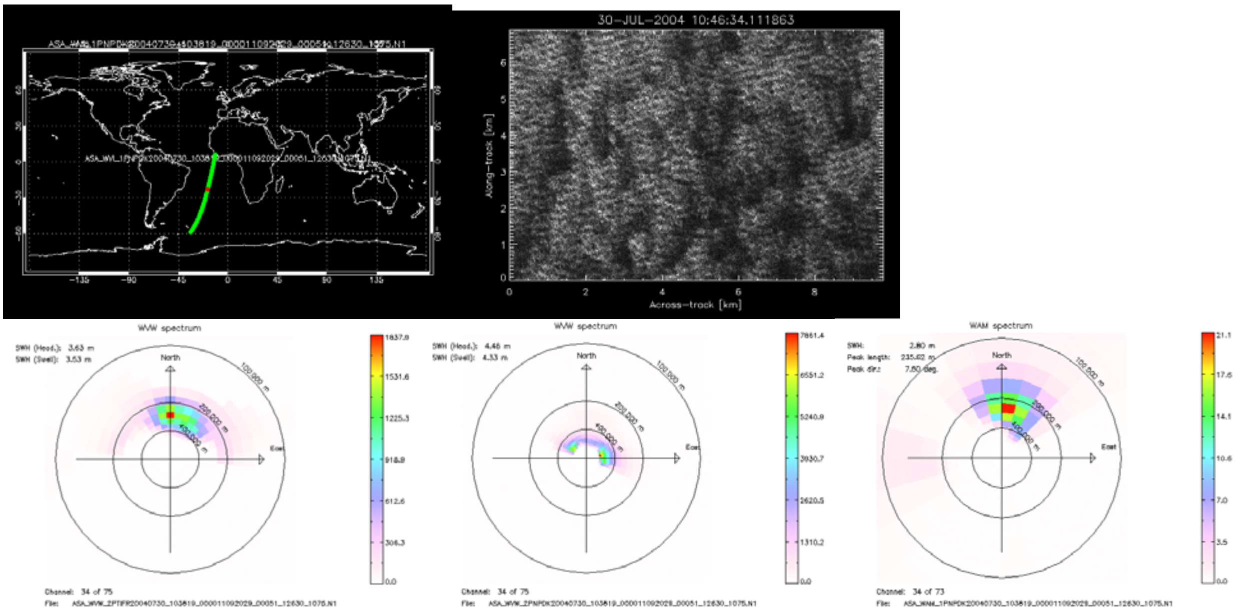

Figure 8: Upper left: imagette location. Upper right: imagette backscatter. Lower left: inverted wave spectrum (new version) . Lower mid: inverted wave spectrum (old version). Lower right: collocated wave model spectrum

To summarize, the following upgrades of the ASAR Wave Mode WVW product and algorithm are implemented in the reprocessing chain at IFREMER [B-9].

a) implementation of a noise correction procedure to apply on the image intensity

b) increased dynamic range of look-up table

c) a new approach for estimation of azimuth cut-off

d) a spectral based low frequency removal procedure implemented

e) improved propagation ambiguity removal

f) improvement of transfer function at low frequencies

The methodology and the results of the validation are described in the following.

4.1 VALIDATION

In the following a geophysical validation is performed over several months of data from year 2004. The ASAR WM data are collocated globally with numerical wave model (WAM/ECMWF) as well as locally with NDBC buoys from Central Pacific, US and Canada west coast and East Coast of US and Canada.

Example of triple collocation and corresponding wave spectra are shown in Figure 9.

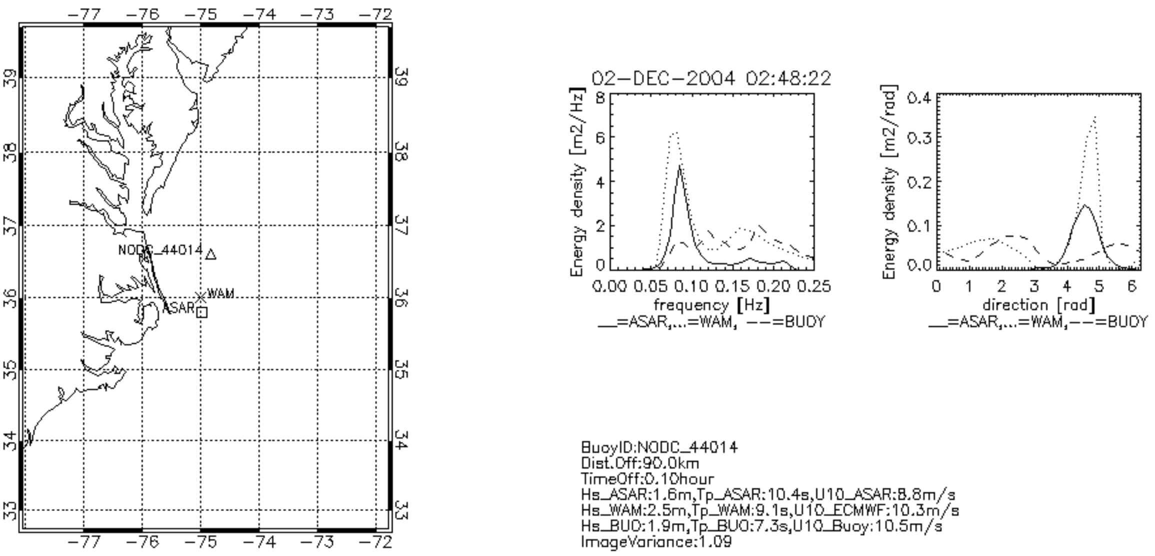

Figure 9: Example of tripple collocation (left) of ASAR WM, ECMWF WAM, and NODC buoy, and the corresponding heave and directional wave spectra (right).

1.4.2 GEOPHYSICAL VALIDATION

The validation consist of intercomparison of wave spectral parameters derived from the various sources (ASAR, NDBC buoys, WAM), followed by an estimation of RMS error and bias. The wave spectral parameters of particular interest is the wave period, $\mathrm{T_p}$, the significant waveheight, $\mathrm{H_s}$, and the wave direction, Φ_p, which are derived from the two-dimensional wave spectra as described in the following. The ASAR Wave Mode Level 2 spectra are given on log-polar grid in wavenumber and direction domain, $F(k,\varphi)$ [B-10]. Note that the ASAR spectrum is in general not the total ocean wave spectrum, but only the wave spectrum within the SAR imaging domain. The size of this domain is again dependent on the azimuth cut-off which again is dependent on the sea state. The frequency-, $F(f)$ and directional spectra, $\psi(\varphi)$ are then derived from the Level 2 spectra, $F(k,\varphi)$ according to the formulas:

$$(1) \qquad F(f) = \int F(k,\varphi) k \cdot dkdf \cdot d\varphi$$

$$(2) \qquad \psi(\varphi) = \int F(k,\varphi) dk$$

$$(3) \qquad \phi(f) = \tan^{-1}\left(\frac{\int F(k,\varphi)\sin\varphi d\varphi}{\int F(k,\varphi)\cos\varphi d\varphi} \right)$$

where $dkdf = 4\pi\sqrt{k/g}$. The significant waveheights, H_s, H_s^{12} mean periods, T_p, T_p^{12}, and mean wave direction, Φ are then computed as:

$$(4) \qquad H_s = 4\sqrt{\int_{f_{\min}}^{f_{\max}} F(f)df}, \qquad H_s^{12} = 4\sqrt{\int_{f_{\min}}^{1/12} F(f)df}$$

(5) $$T_p = \frac{\int_{f_{\min}}^{f_{\max}} F(f) f^{-1} df}{\int_{f_{\min}}^{f_{\max}} F(f) df}, \quad T_p^{12} = \frac{\int_{f_{\min}}^{1/12} F(f) f^{-1} df}{\int_{f_{\min}}^{1/12} F(f) df}$$

(6) $$\Phi = \tan^{-1}\left(\frac{\int_{f_{\min}}^{f_{\max}} F(f) \sin(\phi(f)) df}{\int_{f_{\min}}^{f_{\max}} F(f) \cos(\phi(f)) df} \right)$$

where $f_{\min}, f_{\max}$ are the lowest and highest frequencies in the spectrum to be computed over. Similar parameters can be derived from the co-located WAM and buoy spectra. Spectral peak period, T_{peak} and direction, Φ_{peak}, given as the peak of $F(f)$ and $\psi(\varphi)$, respectively, are also computed and compared. The wave directions are always clock-wise from north towards the direction the waves propagate.
The H_s^{12}, Φ^{12} and T_p^{12} are computed for waves with period longer than 12 sec, which in most cases are longer than then the azimuth cut-off period.

Significant Waveheight:

Comparison of the ASAR significant waveheight of the old (first version) WVW product with the WAM spectra, showed RMS error and bias 0.6m and 0.3m, globally for H_s^{12}. The bias in H_s^{12} showed also strong geographical dependency, 0.2m in the Central and West-Pacific and 0.7m in the East-Atlantic US coast [B-8]. The deviations in significant waveheight also show a clear dependency with wind speed, even for H_s^{12} at low wind speeds. The results of the significant waveheight analysis of the new processing are shown in Figure 10.

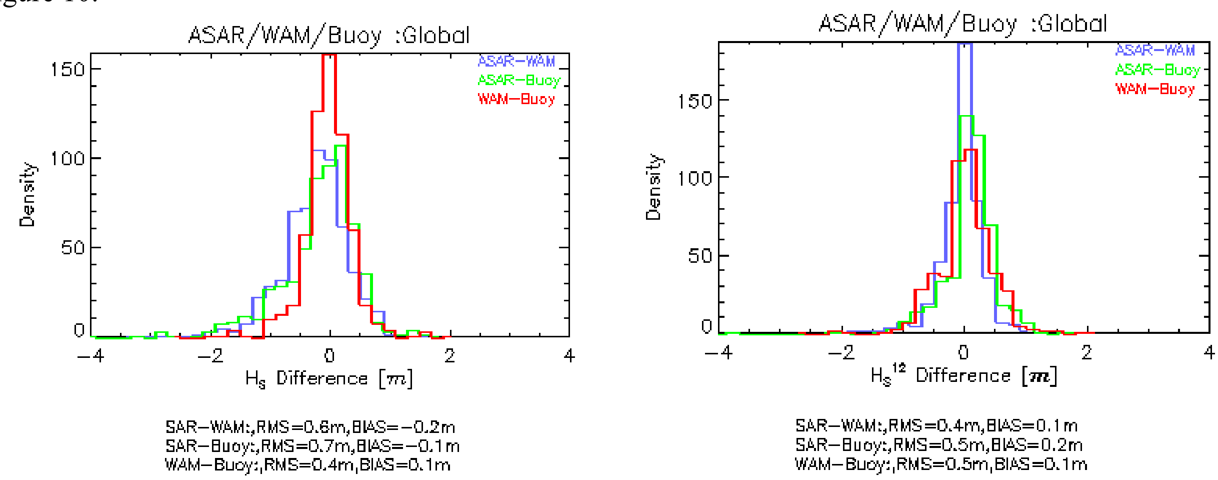

Figure 10: Comparison of significant waveheight from ASAR WVW, WAM and buoy for May, September, and December 2004. The ASAR WM data are processed with the upgraded Level 2 processor at IFREMER.

Figure 10 shows that the bias in H_s^{12}, with the new Level 2 processing, is reduced to only 0.1m as compared to WAM. The geographical dependency in the H_s^{12} bias is also significantly reduced, now 0.0m in the

Pacific and 0.2m in the East-Atlantic US Coast. We also see that the Level 2 H_s^{12} RMS (0.5m) and bias (0.2m) compared to the buoy are comparable with the corresponding values for the WAM (rms=0.5m, bias=0.1m) versus buoy.
If we go global for the waveheight analysis we get the Level2 and WAM scatterplot of $\mathrm{H_s}$ and H_s^{12} as shown in Figure 11.

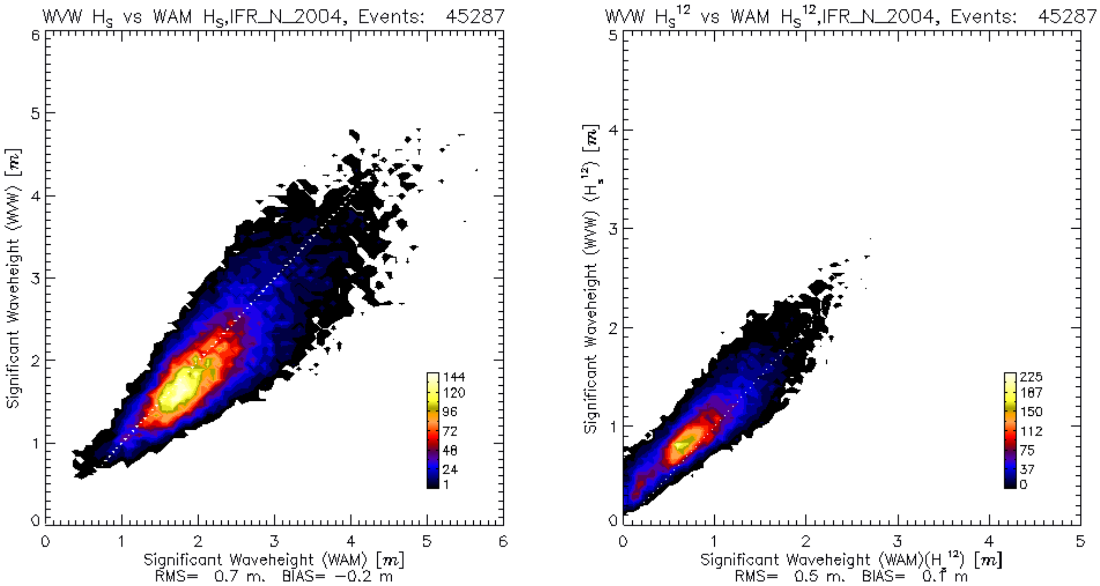

Figure 11: Scatterplot of reprocessed ASAR WVW versus WAM $\mathrm{H_s}$ (left) and H_s^{12} (right) from global data set comprising 45287 collocated spectra.

Figure 11 shows that the global data set verifies the findings from the regional triple collocation data set shown in Figure 10.

In Figure 12 we show the improvements in the $\mathrm{H_s}$ and H_s^{12} bias as function of wind speed for the new Level 2 processing.

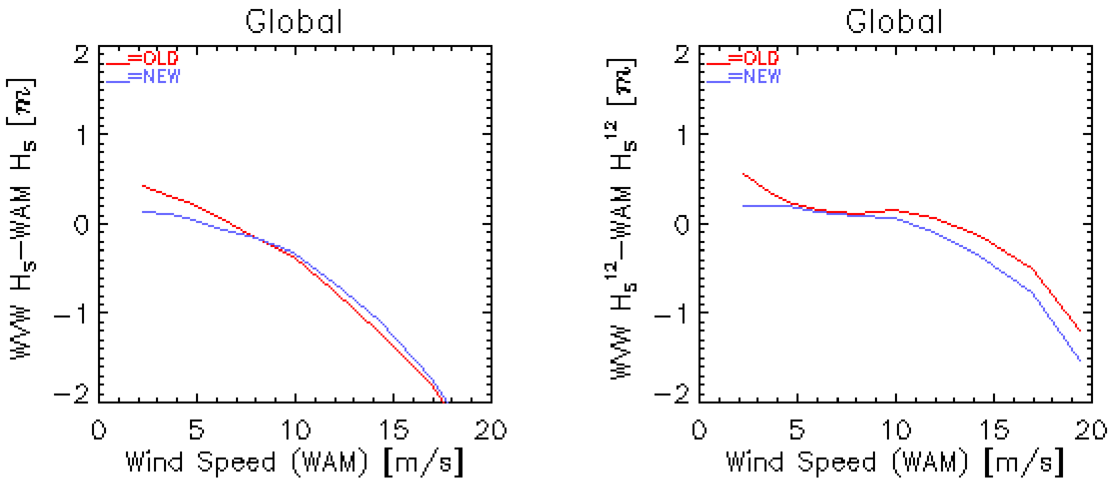

Figure 12: Mean difference in $\mathrm{H_s}$ and H_s^{12} between ASAR WVW and WAM as function of wind speed, for the old Level 2 processing (red) and the new Level 2 processing (blue).

Figure 12 shows that the wind speed dependency in the significant waveheight bias at low wind speed is reduced significantly, and for the swell part almost no dependency is observed for wind speeds below 10m/s. For higher wind speeds, a dependency on wind speed is expected even for the swell since then the azimuth cut-off will be in the swell domain.

Mean Wave Period:

Comparison of the ASAR mean wave period from old version of the WVW product with the WAM spectra, showed RMS error and bias of 1.7s and 1.0s for T_p^{12}, globally. The bias in T_p^{12} showed also strong geographical dependency, 0.7s in the Pacific and 2.6s in the East-Atlantic US coast [B-8]. The result of the mean period analysis is shown in Figure 13.

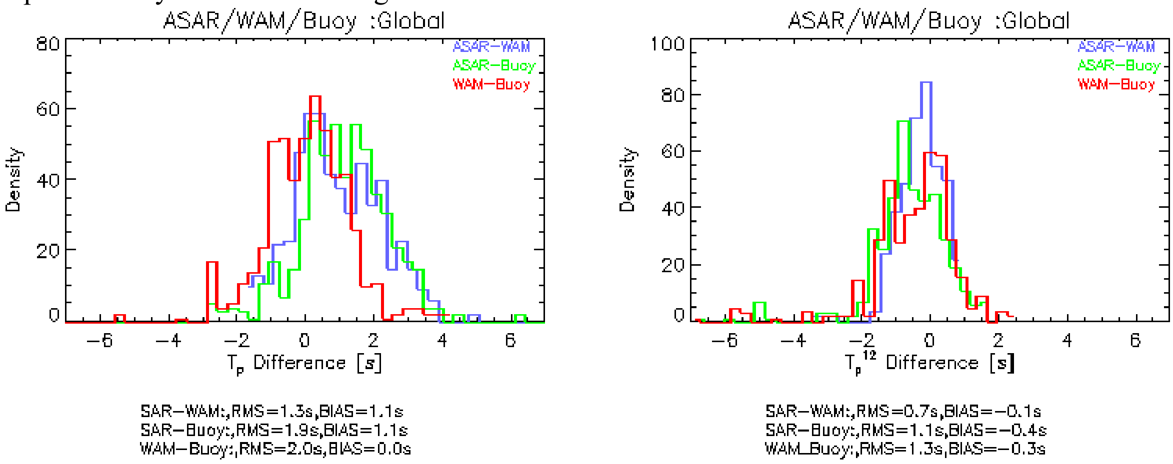

Figure 13: Comparison of mean wave period from ASAR WVW, WAM and buoy for May, September, and December 2004. The ASAR WM data are processed with the upgraded Level 2 processor at IFREMER.

Figure 13 shows that the bias in Level 2 T_p^{12}, with the new processing, is reduced to –0.1s as compared to WAM. The geographical dependency in the T_p^{12} bias is also significantly reduced, now -0.1s in the Pacific and 0.1s in the East-Atlantic US Coast. We also see that the Level 2 T_p^{12} bias (-0.4s) and RMS error (1.1s) compared to the buoys are comparable with the corresponding values for the WAM (bias=-0.3s and rms=1.3s) versus buoy.
The corresponding global results for the wave period are shown in the ASAR WVW and WAM scatterplot shown in Figure 14.

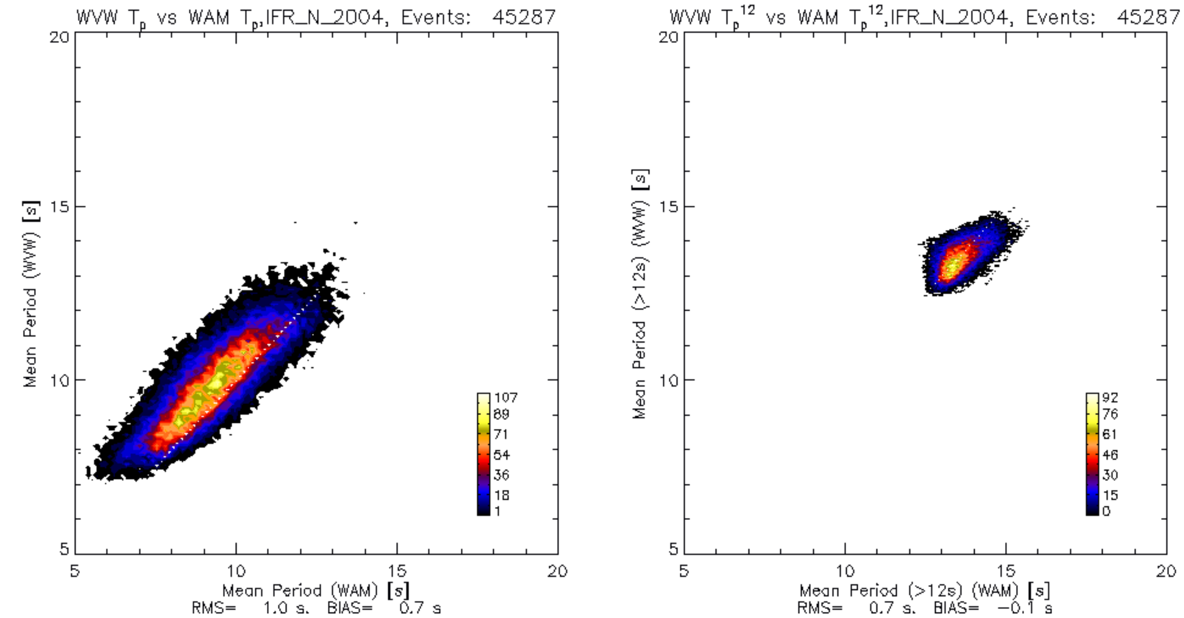

Figure 14: Scatterplot of reprocessed ASAR WVW versus WAM T_p (left) and T_p^{12} (right) from global data set comprising 45287 collocated spectra.

Figure 14 shows that the global data set verifies the findings from the regional triple collocation data set shown in Figure 13.

Wave Direction:

Comparison of the ASAR mean wave direction, Φ^{12} from old version of the WVW product with the WAM spectra, showed RMS error of around 1.15 rad and a bias of 0.35 rad. Unfortunately, the directional informations from buoys are so far limited, so the comparison is only done against WAM data. In Figure 15 (left) we show the results of the comparison of WVW and WAM mean wave direction, while in Figure 15 (right) we show the same for the peak wave direction.

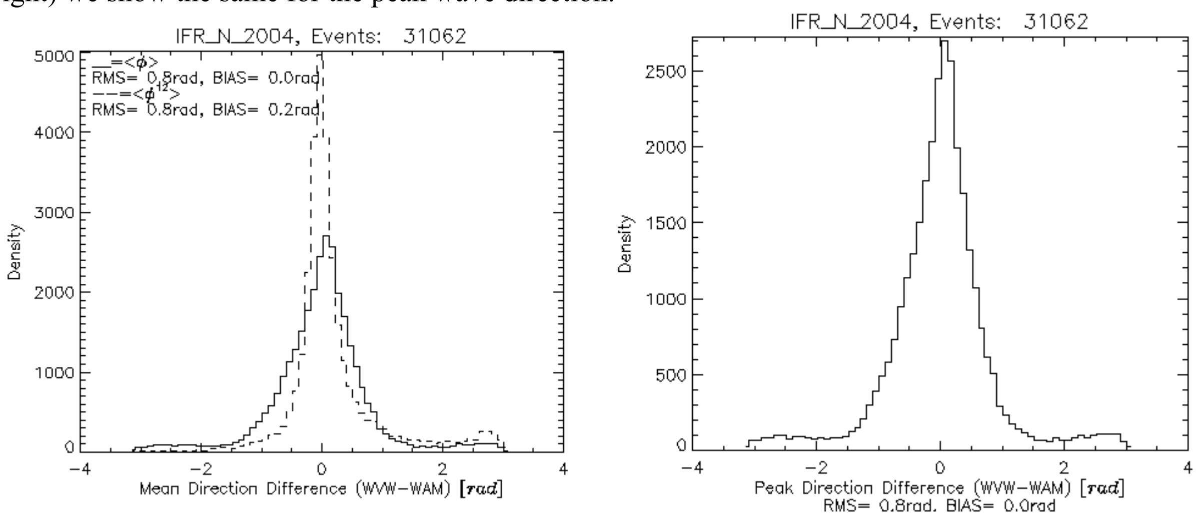

Figure 15: Left: Histogram of mean wave propagation direction difference between ASAR WVW and WAM. Right: Histogram of peak wave direction difference between ASAR WVW and WAM.

Figure 15 (left) shows that mean wave propagation direction RMS difference between ASAR and WAM is reduced from 1.15 rad to 0.8 rad with the new processing, while the bias is reduced from 0.35rad to 0.2 rad, both for the Φ^{12} parameter.
The corresponding scatterplots for ASAR WVW and WAM mean wave period are shown in Figure 16. An improvement of the wave direction can further be achieved by using the ambiguity confidence measure (see Chapter 1.4.3).

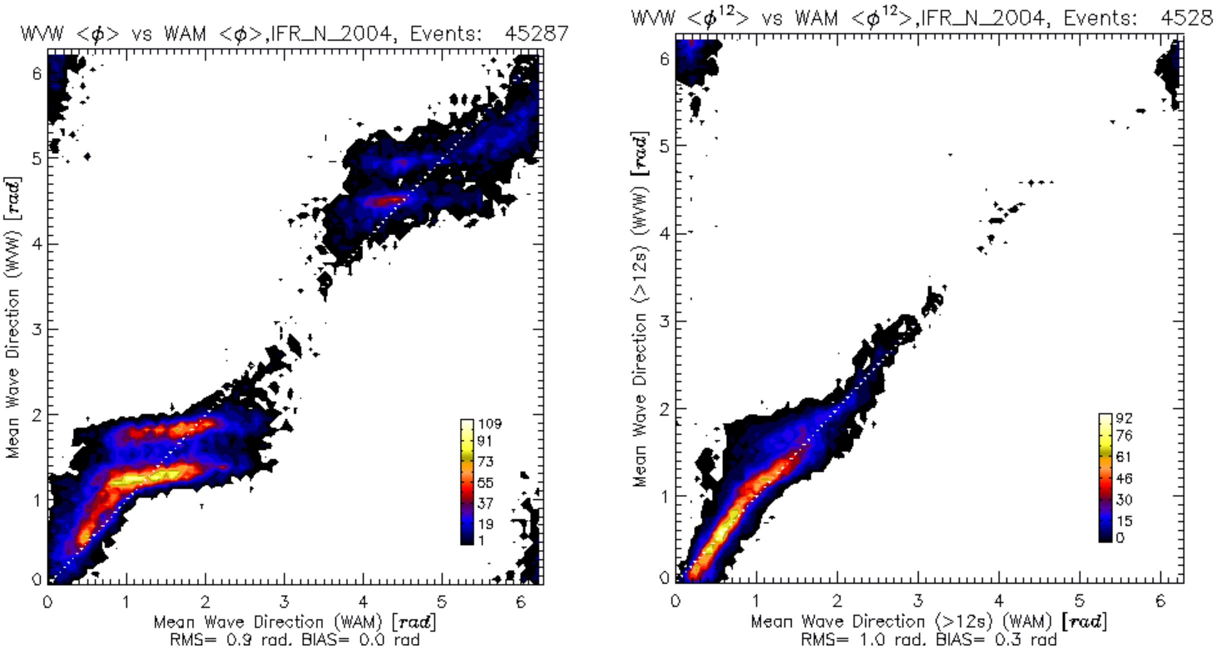

Figure 16: Scatterplot of reprocessed ASAR WVW versus WAM Φ (left) and Φ^{12} (right) from global data set comprising 45287 collocated spectra.

1.4.3 CONFIDENCE PARAMETER

A new confidence parameter (*ambiFac*) was established and included in the header of the new ASAR WVW product. This parameter is useful for assessing the propagation ambiguity in the derived wave spectra. The propagation direction is resolved by using the information in the imaginary part of the cross-spectra. However, for low SNR, a 180 degree ambiguity in the final wave spectra can occur. In order to filter out these data in further use and analysis of the data, the new confidence parameter can be used. In the figures below, we have quantified the impact on the RMS and bias values by using the confidence parameter in the new ASAR WVW product, to exclude ambiguity data from the analysis.
The ambiguity parameter used is stored in one of the spare fields of the new WVW product header. In Figure 17 it is plotted against the swell wave direction difference between WVW and WAM. Figure 17 is then used to define the threshold to filter out the ambiguity SAR spectra.

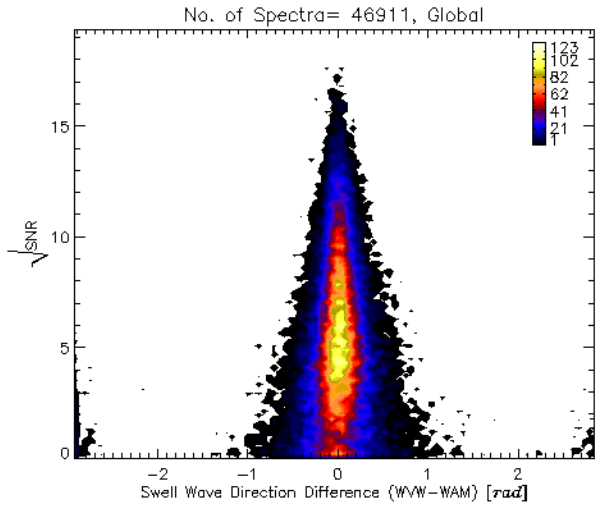

Figure 17: Ambiguity (SNR) as function of swell wave direction difference between ASAR WVW and WAM spectra.

Figure 17 shows that swell wave direction difference between ASAR WVW and WAM spectra increases with decreasing SNR, and that a threshold can be established to filter out ambiguity data. For the analysis shown in Figure 18 (right) we used the threshold $\sqrt{\mathrm{SNR}} = 3$, i.e. disregarding all data with values below this threshold. The thresholding reduces the overall number of data points from 46911 to 31901.

In Figure 18, 19 and 20 we show the impact of using the ambiguity flag on the significant waveheight, mean wave period, and mean wave direction.

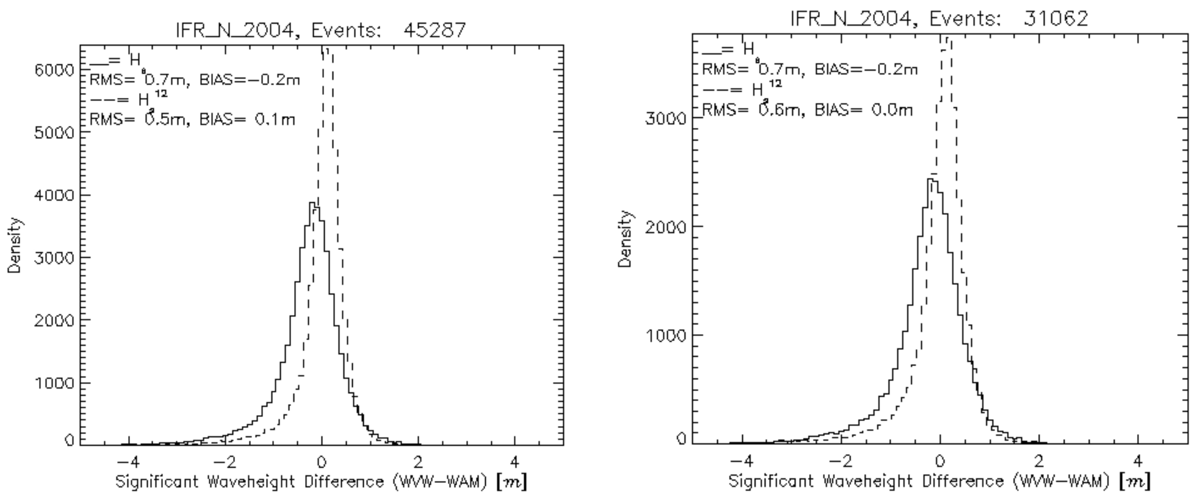

Figure 18: Histogram of difference in significant waveheight between ASAR WVW and WAM without (left) and with (right) ambiguity flagging of data.

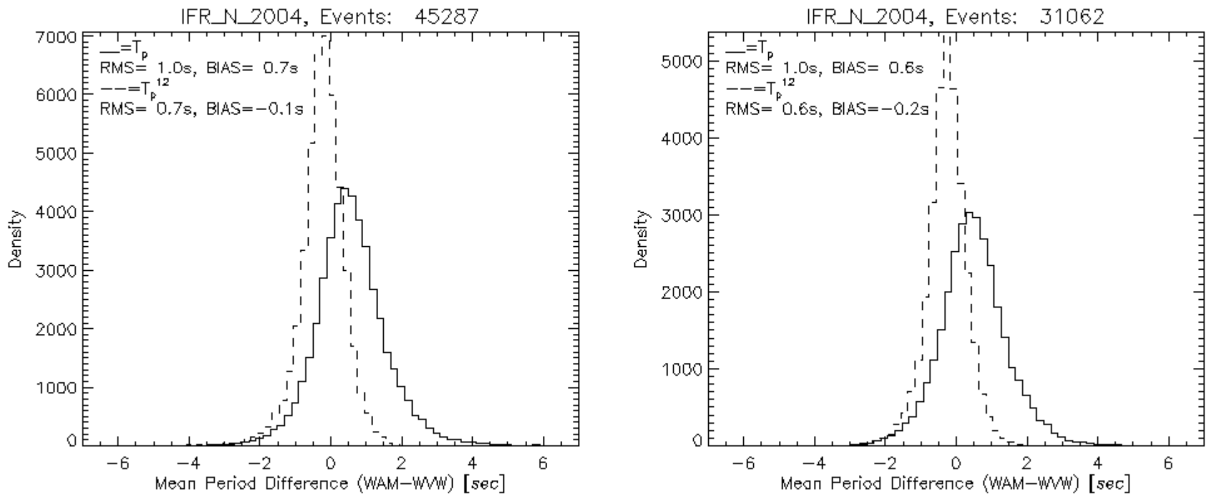

Figure 19: Histogram of difference in mean wave period between Level 2 and WAM without (left) and with (right) ambiguity flagging of data.

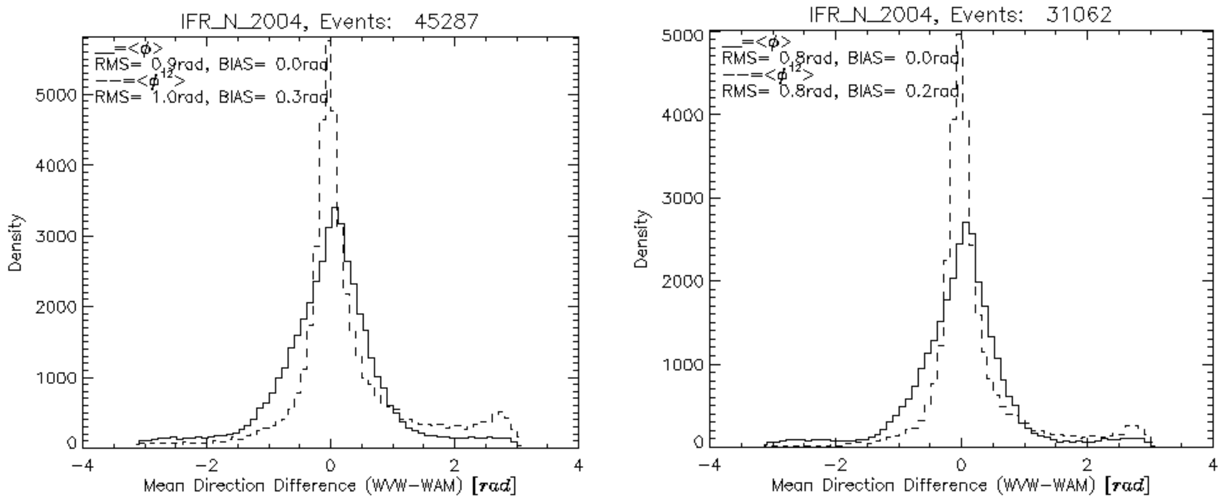

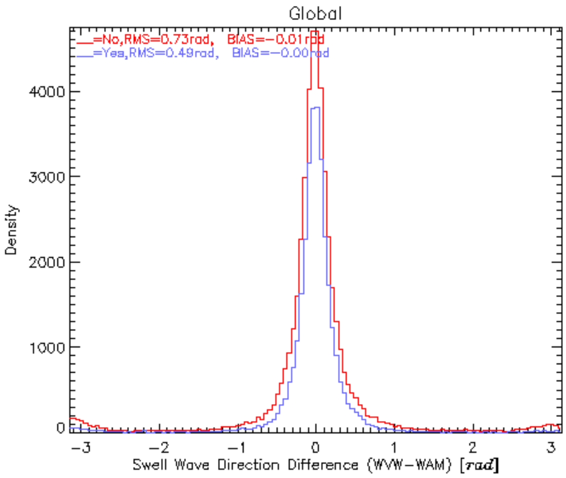

Figure 20: Histogram of difference in mean wave direction between Level 2 and WAM without (upper left) and with (upper right) ambiguity flagging of data. Lower left: Swell wave direction difference between Level 2 and WAM without (red) and with (blue) ambiguity flagging.

We see from Figure 18, 19 and 20 that by using the ambiguity flagging improves the data. Largest improvement is observed for the wave direction, which was also expected.

1.4.4 COMPARISON WITH ORIGINAL ESA PRODUCT

In order to assess the performance of the upgraded ASAR WVW product with respect to the first version of the product, we have generated some plots showing the difference and improvements.

Azimuth Cut-Off:

In Figure 21, we compare the azimuth cut-off parameter before and after the upgrade, and in Figure 22 we illustrate the global correlation between the new azimuth cut-off and the WAM model predicted wind field.

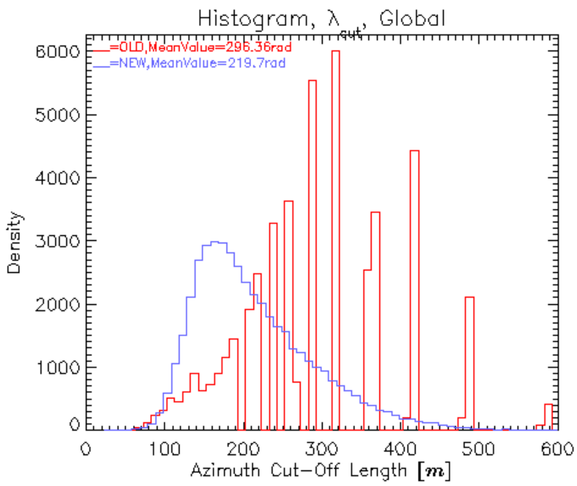

Figure 21: Histogram of azimuth cut-off from the ASAR WM Level 2 product, before (red) an after (blue) the algorithm upgrade.

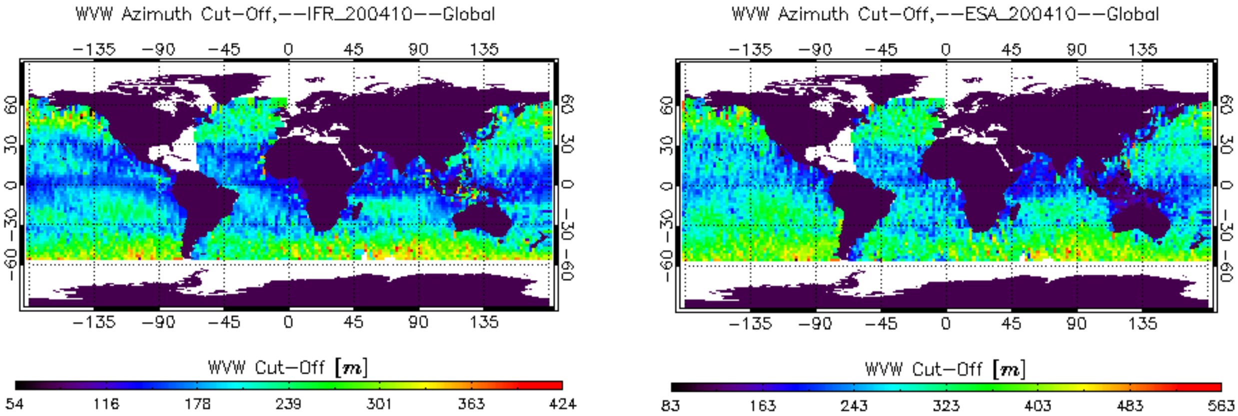

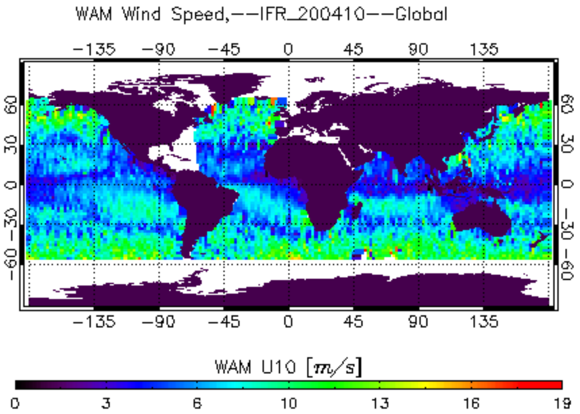

Figure 22: Global maps of azimuth cut-off from upgraded Level 2 product (upper left), old Level 2 product (upper right), and wind speed from ECMWF atmoshperic model (lower left)

Figure 21 and Figure 22 show a significant improvement in the azimuth cut-off from the ASAR WVW product. The histogram is now as expected, and better global correlation with the wind field is also achieved.

Significant Waveheight:

In Figure 23 we show the histogram of the difference in significant waveheight, H_s^{12} and swell significant waveheight between the Level 2 and the WAM before and after the upgrade of the algorithm.

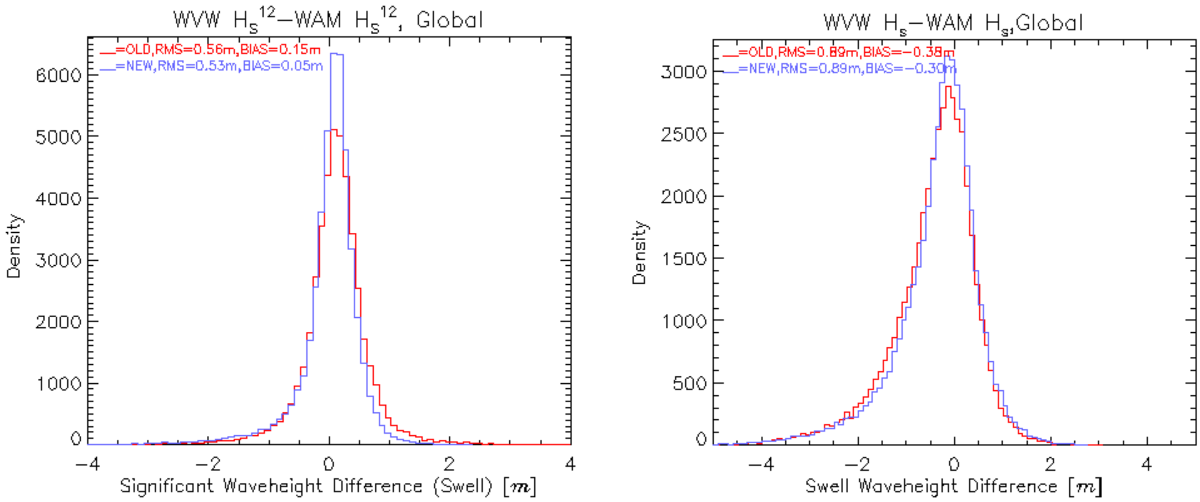

Figure 23: Left: Histogram of difference in significant waveheight between ASAR Level 2 and ECMWF WAM for waves with period longer than 12 sec. Right: Histogram of difference in significant waveheight of the swell between ASAR Level 2 and ECMWF WAM. The red line is the old version of the Level 2 product, while the blue line is the new version.

Figure 23 shows that the bias between ASAR WVW and WAM in significant waveheight is reduced from 0.15m to 0.05m by the new Level 2 processing for $\mathrm{H}_\mathrm{s}^{12}$, and from 0.38m to 0.30m for the swell waveheight. A slight reduction in the RMS error of $\mathrm{H}_\mathrm{s}^{12}$ is also observed for the new ASAR WVW product.

Mean Wave Period:

Figure 24 shows the difference in the mean wave period $\mathrm{T}_\mathrm{p}^{12}$ and swell wave length between ASAR WVW and WAM, before and after the upgrade of the Level 2 processing.

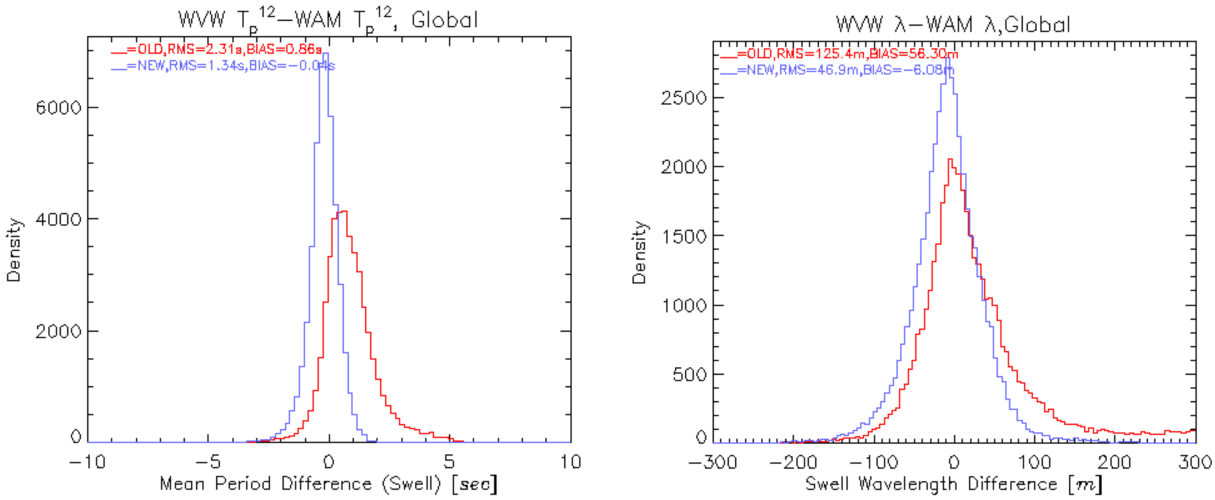

Figure 24: Left: Histogram of difference in mean wave period between ASAR Level 2 and ECMWF WAM for waves with period longer than 12 sec. Right: Histogram of difference in mean wavelength of swell between ASAR Level 2 and ECMWF WAM. The red line is the old version of the Level 2 product, while the blue line is the new version.

Figure 24 show that the bias between ASAR WVW and WAM in mean wave period is reduced from 0.86s to 0.04s by the new Level 2 processing, and for the swell mean wavelength from 56.3m to –6.1m. A significant reduction in the RMS error is also observed for the new WVW product, from 2.31s to 1.34s for the mean period, and from 124m to 46 m for the swell wavelength.

Mean Wave Direction:

Figure 25 shows the difference in the mean wave direction Φ^{12} and swell wave direction between ASAR WVW and WAM, before and after the upgrade of the Level 2 processing. The ambiguity flagging is not used in these plots.

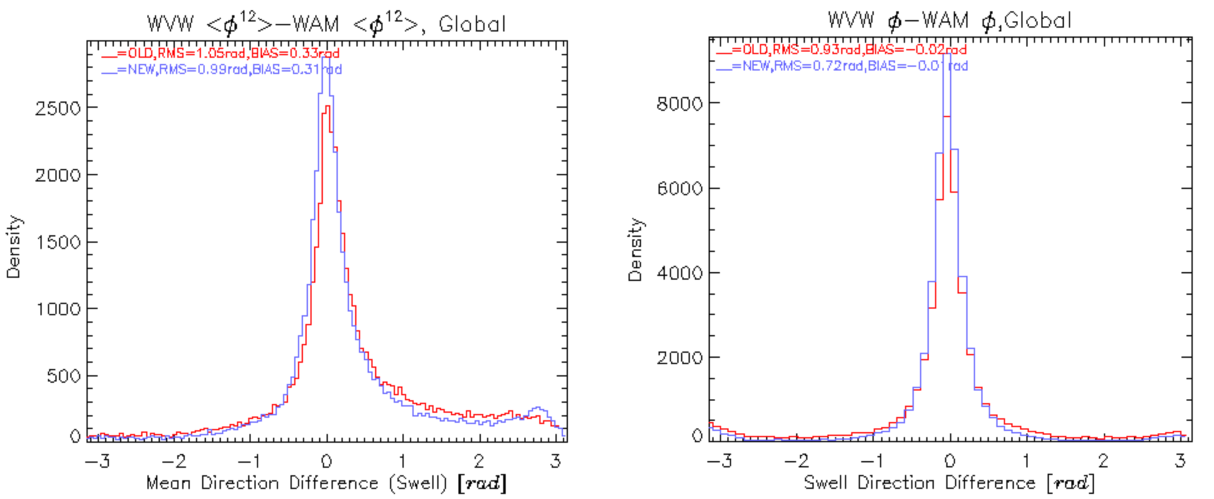

Figure 25: Left: Histogram of difference in mean wave direction between ASAR Level 2 and ECMWF WAM for waves with period longer than 12 sec. Right: Histogram of difference in mean wave direction of swell between ASAR Level 2 and ECMWF WAM. The red line is the old version of the Level 2 product, while the blue line is the new version.

Figure 25 shows only a slight reduction in bias between ASAR WVW and WAM in mean wave direction and swell direction, while a larger reduction in the RMS errors is observed, from 1.05 rad to 0.99 rad for the mean wave direction, and 0.93rad to 0.72 rad from the swell direction.

Wave Age:

A modification of the azimuth cut-off estimation also modified the estimate of the inverse wave age. In Figure 26 we show the difference between wave age before and after the Level 2 algorithm upgrade. We see from Figure 26, a clear improvement in the inverse wave age estimate.

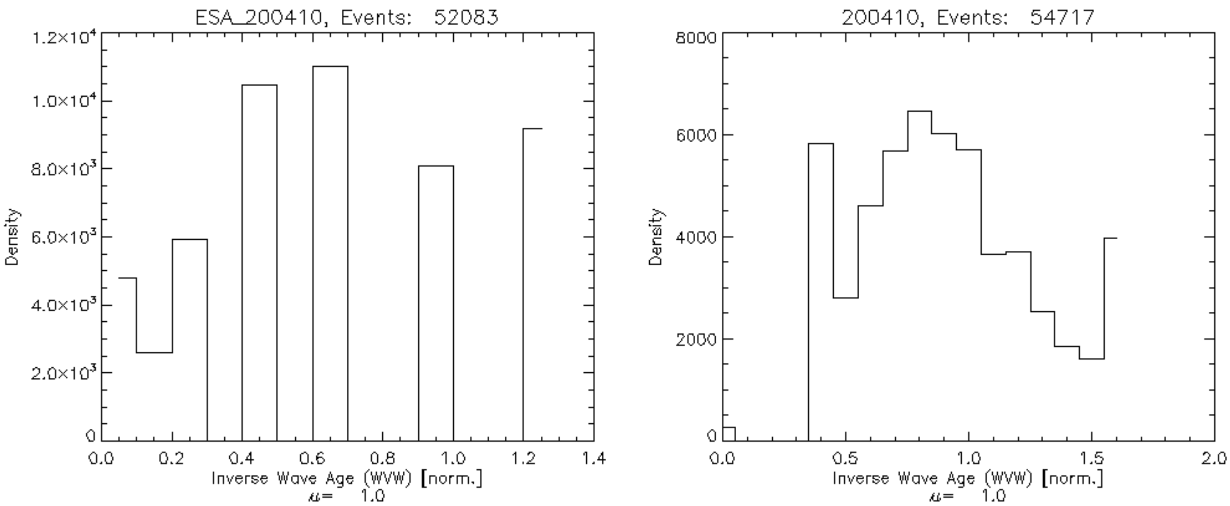

Figure 26: Left: Histogram of inverse wave age from the old ASAR WVW product. Right: Histogram of inverse wave age from the new ASAR WVW product.

1.4.5 TUNING OF PROCESSING SET-UP PARAMETERS

Both the WVS and WVW processing has a set of processing set-up parameters that can be used to tune the output products. For the updated WVS processing, the detrending low pass filter width (trRemWidth, see [A-3]) is of importance. In Figure 27 we show the impact of changing this parameter from 400m to 300m.

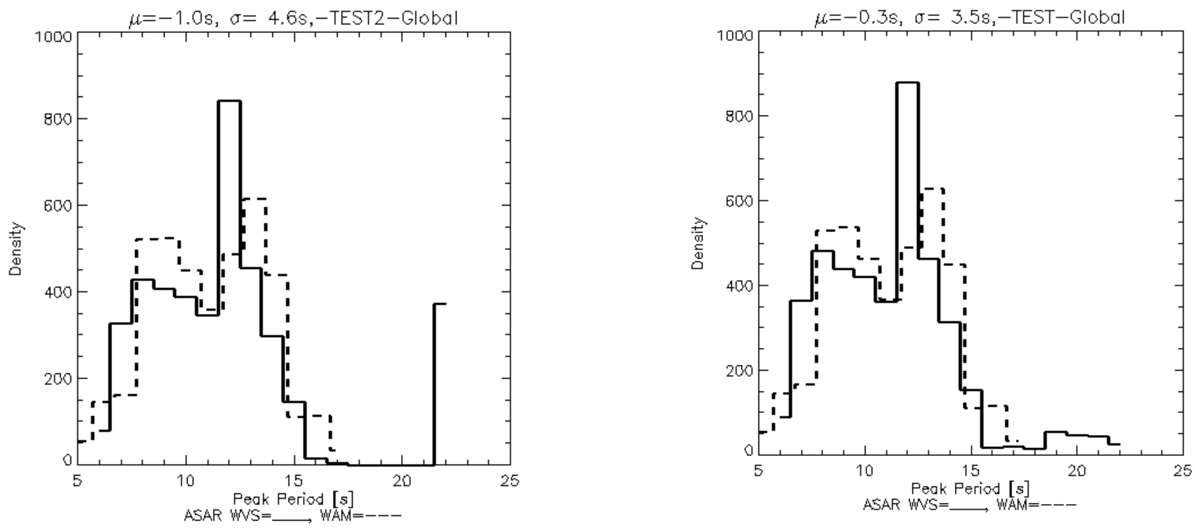

Figure 27: Historam of Peak period of WVS cross spectra and WAM spectra using filter width of 400m (left) and 300m (right).

For the WVW processing, one key parameter to adjust the total energy of the output wave spectra is the MTFThreshold. In Figure 28 we show how this can be used to remove the bias in H_s^{12} as compared to WAM. In the WVW product considered in this validation, we have used set MTFThreshold=0.5 instead of 0.1, which was used for the initial reprocessing and IFREMER.

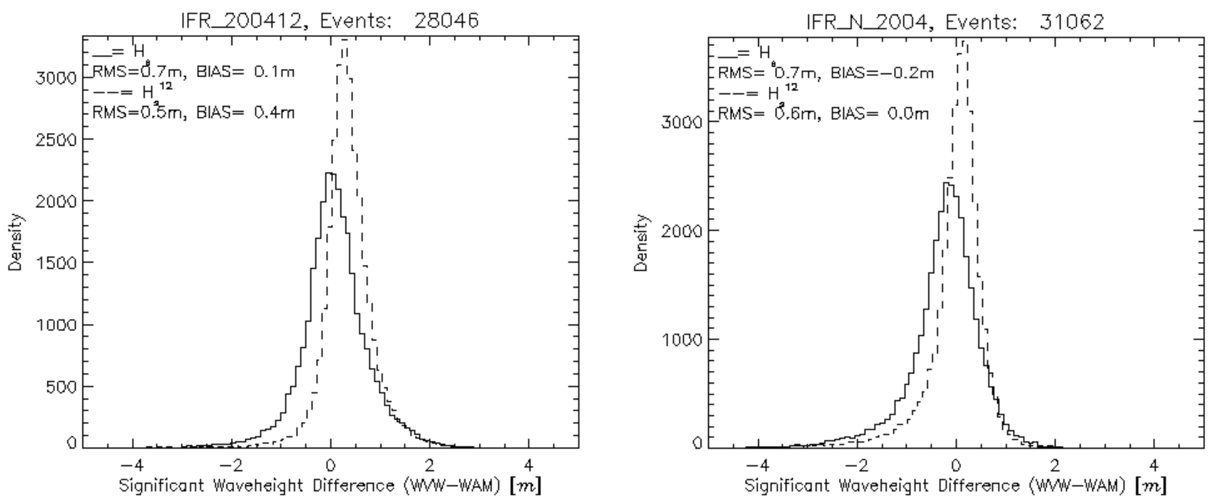

Figure 28: Histogram of H_s and H_s^{12} difference between WVW and WAM using MTFThreshold=0.1 (left) and 0.5 (right).

We see from Figure 28 that by adjusting the MTFThreshold, the bias in H_s^{12} can be removed.

5 CONCLUSIONS

Calibration and validation of the upgraded ASAR WM WVS and WVW products are conducted using collocated WAM model as provided by ECMWF as well as available buoy data. The geophysical validation consist of systematic regional comparison with collocated wave parameters of the WAM model. Validation of the upgraded processing shows a significant improvement in the geophysical quality of the both the WVS and the WVW product. Less RMS deviation and bias between WVW and WAM or buoy wave spectra parameters are observed. We now observe that the RMS and bias of H_s^{12} and $\mathrm{T}_\mathrm{p}^{12}$ of the WVW is similar to values of WAM, both compared to the buoys. For H_s^{12} these are 0.5m and 0.2m, and for $\mathrm{T}_\mathrm{p}^{12}$ these are 1.1s and -0.4s. For the mean wave propagation direction Φ^{12} we observe and RMS error and bias of 45° and 11°, while considering the swell we have an RMS error of 27° and no bias.

We also see that more of the WM data gives meaningful wave spectra, and an improved flagging of ambiguity data is achieved as well the number of products passing the quality control. The latter is of importance for the assimilation of WVW products into NWP models.